PHYSICAL REVIEW LETTERS **120,** 244101 (2018)

Kuramoto Model for Excitation-Inhibition-Based Oscillations

Ernest Montbrió[1] and Diego Pazó[2]
[1]*Center for Brain and Cognition. Department of Information and Communication Technologies, Universitat Pompeu Fabra, 08018 Barcelona, Spain*
[2]*Instituto de Física de Cantabria (IFCA), CSIC-Universidad de Cantabria, 39005 Santander, Spain*

(Received 4 January 2018; revised manuscript received 10 April 2018; published 13 June 2018)

The Kuramoto model (KM) is a theoretical paradigm for investigating the emergence of rhythmic activity in large populations of oscillators. A remarkable example of rhythmogenesis is the feedback loop between excitatory (E) and inhibitory (I) cells in large neuronal networks. Yet, although the EI-feedback mechanism plays a central role in the generation of brain oscillations, it remains unexplored whether the KM has enough biological realism to describe it. Here we derive a two-population KM that fully accounts for the onset of EI-based neuronal rhythms and that, as the original KM, is analytically solvable to a large extent. Our results provide a powerful theoretical tool for the analysis of large-scale neuronal oscillations.

DOI: 10.1103/PhysRevLett.120.244101

The Kuramoto model (KM) is an idealized mathematical model for exploring the birth of collective synchronization in its most simple form. It consists of a population of heterogeneous, all-to-all coupled oscillators, and is a unique example of an exactly solvable system of nonlinear differential equations [1–5]. Yet, the KM was originally not intended as a specific description of any particular system, and finds limited applications in the modeling and analysis of natural oscillatory phenomena, see, e.g., Refs. [6–8].

An important example of collective synchronization is that of large scale neuronal oscillations [3,9]. Despite continued work using the KM to investigate neuronal rhythms (see, e.g., Refs. [10–16]), it remains unknown whether the KM actually accounts for the neuronal mechanisms resulting in such oscillations. In this Letter we derive a simple, two-population KM, that describes one of the basic mechanisms of generation of neuronal oscillations: The feedback loop between fast excitation (E) and slow inhibition (I) in large neuronal networks [17–20].

EI-feedback loop and EI-based oscillations.—The canonical neuronal network to model the EI-feedback loop consists of two interacting populations of excitatory and inhibitory neurons [21–24]. Here, we consider two populations of N pulse-coupled “Winfree oscillators” [2,25–29] with phase variables $\{\theta_i^\sigma\}_{i=1,\ldots,N}$ (populations are identified by $\sigma \in \{E, I\}$), which evolve according to

$$\dot{\theta}_i^\sigma = \omega_i^\sigma + \xi_i^\sigma + Q(\theta_i^\sigma)(K_{\sigma E} h_E - K_{\sigma I} h_I). \tag{1}$$

The natural frequencies ω_i^σ are drawn from Lorentzian distributions of half-width γ, centered at $\bar{\omega}_\sigma$

$$g_\sigma(\omega) = (\gamma/\pi)[(\omega - \bar{\omega}_\sigma)^2 + \gamma^2]^{-1}, \tag{2}$$

and ξ_i^σ are independent, zero-mean delta-correlated noise processes of strength D: $\langle \xi_i^\sigma(t) \xi_j^{\sigma'}(t') \rangle = 2D\delta(t-t')\delta_{i,j}\delta_{\sigma,\sigma'}$. In Eq. (1), $Q(\theta)$ is the so-called phase response curve (PRC) that determines the response of the oscillators to perturbations. Here we adopt the (infinitesimal) PRC of the theta-neuron model, $Q(\theta) = 1 - \cos\theta$, which is non-negative and thus results in phase advances or delays in response to excitatory or inhibitory inputs [30–32]. Neuronal oscillators with a non-negative PRC are called Type 1, and include a broad class of neuronal models, see, e.g., Refs. [31–33]. The oscillators interact all-to-all via the mean fields

$$h_\sigma = \frac{1}{N} \sum_{j=1}^{N} P(\theta_j^\sigma), \tag{3}$$

which are population-averaged sums of all the pulses P produced in each population. We use the family of unimodal even-symmetric functions $P(\theta) = (1-r)(1+\cos\theta)(1 - 2r\cos\theta + r^2)^{-1}$, with $\int_{-\pi}^{\pi} P(\theta) d\theta = 2\pi$ and a free parameter $r \in (-1, 1)$, such that $\lim_{r\to 1} P(\theta) = 2\pi\delta(\theta)$ [28]. Expressed in words, the jth oscillator in the E population exerts a positive, pulselike influence $P(\theta_j^E)$ of strength $K_{EE}/N \geq 0$ to each oscillator of the E population, and of strength $K_{IE}/N \geq 0$ to each oscillator of the I population [similarly for the jth oscillator of the I population, with an explicit “$-$” sign in Eq. (1) corresponding to inhibition].

Figures 1(a) and 1(b) show EI-based oscillations of the mean-field quantities h_σ in simulations of (a) heterogeneous and (b) noisy EI-Winfree networks, Eq. (1). The raster plots Figs. 1(c) and 1(d) show that an EI-oscillation cycle begins with the synchronous “firing” of a large cluster of phase-locked E oscillators, followed by another synchronous firing of the I oscillators. Note that, to emphasize that oscillations emerge exclusively due to the interplay between fast excitatory and slow inhibitory dynamics, in

0031-9007/18/120(24)/244101(6)

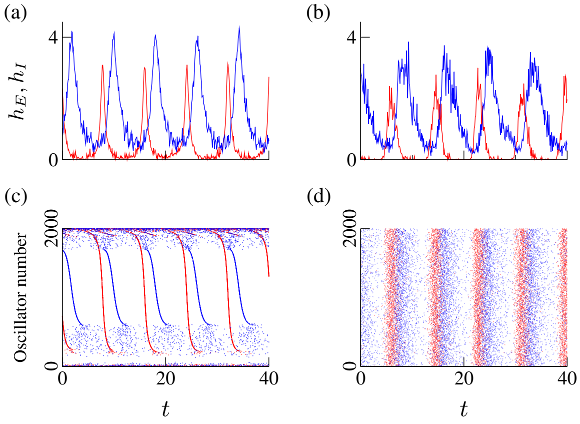

FIG. 1. *EI*-based oscillations in a population of $N = 2000$ excitatory (E) and $N = 2000$ inhibitory (I) Winfree oscillators, Eq. (1); with $\bar{\omega}_E = 1.5$, $\bar{\omega}_I = 0.5$, $K_{EI} = K_{IE} = 0.5$, $K_{EE} = K_{II} = 0$, and $r = 0.99$. (a), (b) Time series of the E (red) and I (blue) activity-based mean fields h_σ. (c), (d) Raster plots: A point is plotted when an oscillator's phase reaches a multiple of 2π, which is the peak location of $P(\theta)$. In (a) and (c) frequencies are Lorentzian distributed, with $\gamma = 0.1$, and $D = 0$. In (b) and (d) the noise strength is $D = 0.1$, and $\gamma = 0$.

Fig. 1 we set the self-coupling terms to zero, $K_{EE} = K_{II} = 0$, and consider $\Delta\omega \equiv \bar{\omega}_E - \bar{\omega}_I > 0$. In the following we derive a two-population KM that captures the main features of the oscillations shown in Fig. 1, and that is exactly solvable to a large extent.

Excitation-inhibition Kuramoto model (EI-KM).—Invoking the averaging approximation, valid for weak coupling and nearly identical oscillators [1,3], the *EI*-Winfree model in Eq. (1) reduces to the *EI*-KM [34]

$$\dot{\theta}_i^\sigma = \tilde{\omega}_i^\sigma + \xi_i^\sigma - \frac{1+r}{2N}\sum_{j=1}^{N}[K_{\sigma E}\cos(\theta_i^\sigma - \theta_j^E) - K_{\sigma I}\cos(\theta_i^\sigma - \theta_j^I)], \quad (4)$$

where $\tilde{\omega}_i^\sigma \equiv \omega_i^\sigma + K_{\sigma E} - K_{\sigma I}$. There are two major differences between the *EI*-KM and the classical two-population KM broadly investigated in the literature, see, e.g., Refs. [1,35–40]. First, in the *EI*-KM the excitatory and inhibitory coupling constants differentially shift the natural frequencies $\tilde{\omega}_i^E$ and $\tilde{\omega}_i^I$, and this largely affects the regions of parameters where *EI* oscillations occur. Second, although the cosine coupling does not promote synchrony in the KM [41], the positive (E) and negative (I) cross-coupling terms in Eq. (4) crucially conspire to synchronize the oscillators [42]. Therefore, in the *EI*-KM, synchrony sets in exclusively due to the cooperative action of both the E and the I populations, in consonance with the *EI*-feedback loop mechanism. Indeed, Fig. 2 shows numerical simulations of the *EI*-KM in Eq. (4) using the same parameters as in Figs. 1(a) and 1(c)—except r, which in the *EI*-KM is set to $r = 1$, see below. Figure 2(a) displays the amplitude of the complex Kuramoto order parameters $Z_\sigma \equiv R_\sigma e^{i\Psi_\sigma} = N^{-1}\sum_{j=1}^{N} e^{i\theta_j^\sigma}$. At $t = 0$, the amplitudes R_E and R_I are near zero since the initial values of all the phases are randomly distributed in the interval $[0, 2\pi)$. Then, after a brief transient, the Kuramoto order parameters converge (up to finite-size fluctuations) to uniformly rotating solutions $Z_\sigma(t) = R_* e^{i\Psi_\sigma(t)}$, with $0 < R_* < 1$ and $\dot{\Psi}_\sigma = \Omega$, signaling the onset of collective synchronization. Note that the raster plot in Fig. 2(b) shows that the cluster of E oscillators precedes the cluster of I oscillators, consistent with Fig. 1(c).

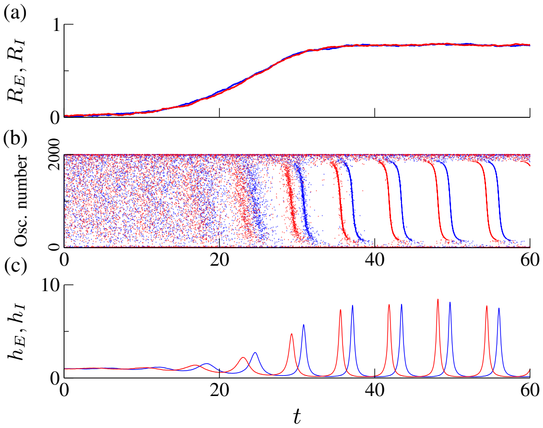

FIG. 2. *EI*-based oscillations in the *EI*-KM Eq. (4) with quenched heterogeneity and $N = 2000$. (a) Amplitude of the Kuramoto order parameters, R_E (red) and R_I (blue); (b) raster plots; (c) mean fields obtained applying Eq. (14) to Z_σ; parameters are as in Figs. 1(a) and 1(c), except that here $r = 1$, instead of $r = 0.99$.

Finally, in the *EI*-KM the width of the pulses (controlled by r) influences the intensity of the cosine coupling functions. To lighten the notation, hereafter we set $r = 1$ in Eq. (4), corresponding to the limit of infinitely narrow (Dirac delta) pulses—this is close to the value used in Fig. 1. The generalization of our results to general r is trivial.

Analysis of the EI-KM.—Equation (4) can be efficiently analyzed in the thermodynamic limit, $N \to \infty$. To do so, the discrete sets of phases and frequencies turn into continuous variables $\{\theta_i^\sigma, \omega_i^\sigma\} \to \{\theta_\sigma, \omega_\sigma\}$, and the corresponding probability density functions $f^\sigma(\theta_\sigma|\omega_\sigma, t)$ satisfy coupled Fokker-Planck equations

$$\partial_t f^\sigma = -\partial_{\theta_\sigma}(f^\sigma \dot{\theta}_\sigma) + D\partial_{\theta_\sigma}^2 f^\sigma, \quad (5)$$

for which the fully incoherent state $f^E = f^I = (2\pi)^{-1}$ is always a trivial solution [35,43]. It is convenient to introduce the Fourier expansion of f^σ:

$$f^\sigma(\theta|\omega, t) = \frac{1}{2\pi}\sum_{l=-\infty}^{\infty} f_l^\sigma(\omega, t)e^{il\theta}, \quad (6)$$

where $f_0^\sigma = 1$ and $(f_{-l}^\sigma)^* = f_l^\sigma$ (the asterisk denotes complex conjugate). Thus, the Kuramoto order parameters are

$$Z_\sigma = \left(\int_{-\infty}^{\infty} f_1^\sigma(\omega, t) g_\sigma(\omega) d\omega \right)^*. \qquad (7)$$

Substituting Eq. (6) into Eq. (5), yields two infinite sets of integro-differential equations for the Fourier modes

$$\dot{f}_l^\sigma = -(il\tilde{\omega}_\sigma + l^2 D) f_l^\sigma + \frac{il}{2} f_{l-1}^\sigma (K_{\sigma E} Z_E^* - K_{\sigma I} Z_I^*) + \frac{il}{2} f_{l+1}^\sigma (K_{\sigma E} Z_E - K_{\sigma I} Z_I), \qquad (8)$$

where $\tilde{\omega}_\sigma \equiv \omega_\sigma + K_{\sigma E} - K_{\sigma I}$. The stability of the incoherent state can be analyzed by linearizing Eq. (8) [44]. To simplify the analysis, we study the case in which cross- and self-couplings are symmetric,

$$K_{EI} = K_{IE} \equiv K, \qquad K_{II} = K_{EE} \equiv \epsilon K, \qquad (9)$$

and use the new parameter $\epsilon \geq 0$ as a measure of the ratio of self- to cross-coupling. Then we find that the eigenvalues determining the stability of incoherence are

$$\lambda_\pm = -\gamma - D \pm \frac{1}{2} \sqrt{K^2 - [\Delta\omega + (\epsilon - 2)K]^2} - i\Omega, \qquad (10)$$

where $\Omega = (\bar{\omega}_E + \bar{\omega}_I)/2$ is the center of the frequency distribution combining E and I populations. Note that parameters γ and D play identical roles in Eq. (10), as it occurs in the KM [40,43]. Imposing $\mathrm{Re}(\lambda_+) = 0$ in Eq. (10), we find the boundary of incoherence

$$\left(\frac{\Delta\omega}{\gamma + D} \right)_c^\pm = (2 - \epsilon) \frac{K}{\gamma + D} \pm \sqrt{\left(\frac{K}{\gamma + D} \right)^2 - 4}, \qquad (11)$$

which is the family of hyperbolas depicted by solid and dashed black lines in Figs. 3(a)–3(d), for increasing values of ϵ. A necessary condition for the boundary Eq. (11) to exist is

$$\frac{K}{\gamma + D} \geq 2. \qquad (12)$$

Hence, given a certain level of heterogeneity and/or noise, synchronization sets in at large enough values of the coupling strength. This is remarkably similar to the KM [1,43], although here K represents cross-, and not self-coupling. Moreover, Eq. (12) is not a sufficient condition for synchronization in the EI-KM. If Eq. (12) is satisfied, then Eq. (11) shows that synchronization is only achieved for a particular range of values of the frequency mismatch $\Delta\omega$. The coupling ratio ϵ does not affect Eq. (12), but it critically controls the range of $\Delta\omega$ for stable incoherence: Note that when $\epsilon \leq 1$, the boundary Eq. (11) is located at positive values of $\Delta\omega$, and thus incoherence is always stable when I oscillators are intrinsically faster than E oscillators ($\Delta\omega < 0$), see Fig. 3. Increasing the parameter ϵ shifts the boundary, with asymptotes at $K = \Delta\omega/(3 - \epsilon)$ and $K = \Delta\omega/(1 - \epsilon)$, towards negative values of $\Delta\omega$. Thus, increasing the coupling ratio through ϵ provides a key ingredient for synchronizing EI networks when $\bar{\omega}_I > \bar{\omega}_E$, as I-to-I coupling slows down I oscillators while E-to-E coupling speeds up E oscillators.

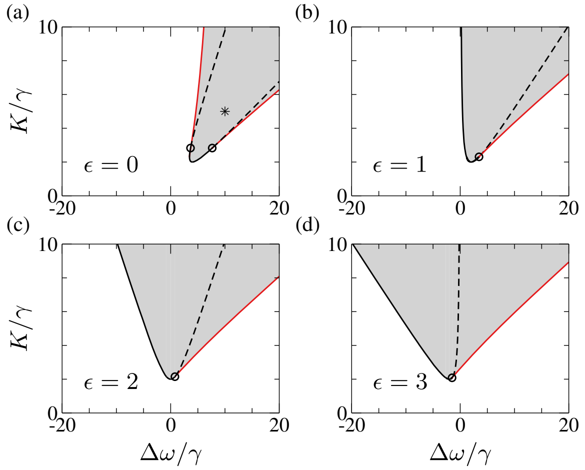

FIG. 3. Phase diagrams of the EI-KM Eq. (4) with $D = 0$ and coupling constants given by Eq. (9), for (a) $\epsilon = 0$, (b) $\epsilon = 1$, (c) $\epsilon = 2$, and (d) $\epsilon = 3$. Regions of stable synchronization are highlighted in gray. Synchronization and incoherence are both stable in regions limited by black-dashed and red lines. The asterisk in (a) marks the parameter values used in Fig. 2. Black lines correspond to Eq. (11). Solid and dashed lines are separated by codimension-2 points—obtained from Eq. (19)—and indicate super- and subcritical bifurcations, respectively. Red curves indicate saddle-node bifurcations.

The synchronization region turns out to be larger than the hyperbolic boundary defined by Eq. (11), particularly for large ϵ values (see Fig. 3 for the noise-free case). The reason is that the bifurcation at Eq. (11) is often subcritical. To investigate this further, next we consider the purely heterogeneous ($D = 0$) and the purely noisy ($\gamma = 0$) cases separately, and show that the global picture is remarkably similar in both instances.

The noise-free problem is particularly simple since it can be assumed that the densities in Eq. (6) satisfy the so-called Ott-Antonsen (OA) ansatz [45,46]

$$f_{l>1}^\sigma(\omega, t) = [f_1^\sigma(\omega, t)]^l. \qquad (13)$$

A first useful outcome of the OA ansatz is that it allows us to infer the mean field h_σ, Eq. (3), from the Kuramoto order parameter Z_σ, Eq. (7). Specifically, in the thermodynamic limit $h_\sigma(t) = \int_{-\infty}^{\infty} \int_0^{2\pi} P(\theta) f^\sigma(\theta|\omega, t) g_\sigma(\omega) d\omega d\theta$. Then, considering $P(\theta)$ as defined above, and the heterogeneity in Eq. (2), one finds $h_\sigma = \mathrm{Re}[(1 + Z_\sigma)/(1 - rZ_\sigma)]$, see Ref. [47]. In the limit $r \to 1$, this relation reduces to

$$h_\sigma = (1 - R_\sigma^2)(1 + R_\sigma^2 - 2R_\sigma \cos\Psi_\sigma)^{-1}. \qquad (14)$$

Figure 2(c) displays the mean fields $h_\sigma(t)$ obtained applying Eq. (14) to the Kuramoto order parameters $Z_\sigma(t)$ of the *EI*-KM. It can be seen that uniformly rotating solutions of the Kuramoto order parameters correspond to pulsatile oscillations of the activity-based mean fields $h_\sigma(t)$ [48]. Though the agreement between Figs. 1(a) and 2(c) is only qualitative, it gradually improves as parameters γ and $\Delta\omega$ are decreased and the averaging approximation becomes more accurate [49].

A major simplification occurs assuming that f^σ evolve in the so-called OA manifold, Eq. (13), as the system of Eq. (8) becomes independent of the index l. Then, solving the integrals in Eq. (7) by virtue of the residue theorem, we find a system of two complex-valued ordinary differential equations for $Z_\sigma(t) = f_1^\sigma(\omega = \bar{\omega}_\sigma - i\gamma, t)^*$

$$\dot{Z}_\sigma = i\left[\hat{\bar{\omega}}_\sigma Z_\sigma - \frac{K_{\sigma E}}{2}(Z_\sigma^2 Z_E^* + Z_E) + \frac{K_{\sigma I}}{2}(Z_\sigma^2 Z_I^* + Z_I)\right], \qquad (15)$$

with $\hat{\bar{\omega}}_\sigma \equiv \bar{\omega}_\sigma + K_{\sigma E} - K_{\sigma I} + i\gamma$. Restricting our analysis to the case defined by Eq. (9), Eq. (15) reduces to a three-dimensional system for the amplitudes R_σ and the phase difference $\Phi \equiv \Psi_E - \Psi_I$. The analysis becomes further facilitated restricting to the symmetric subspace

$$R_E = R_I \equiv R, \qquad (16)$$

in consistency with our numerical observations, the transverse stability of the fixed points [50], and related work [51]. Hence, we analyze the planar system

$$\dot{R} = R\left[-\gamma + \frac{K}{2}(1 - R^2)\sin\Phi\right], \qquad (17a)$$

$$\dot{\Phi} = \Delta\omega + K[(1 + R^2)\cos\Phi - 2 + \epsilon(1 - R^2)]. \qquad (17b)$$

Besides the fixed point at $R_* = 0$, corresponding to incoherence, the nontrivial fixed points of Eqs. (17) satisfy [52]

$$\frac{\Delta\omega}{\gamma} = [2 + \epsilon(R_*^2 - 1)]\frac{K}{\gamma} \pm (R_*^2 + 1)\sqrt{\frac{K^2}{\gamma^2} - \frac{4}{(1 - R_*^2)^2}}. \qquad (18)$$

Figure 4(a) displays R_* obtained from Eq. (18) for $\epsilon = 0$. In this case the transitions to synchronization are hysteretic and the stable synchronized solution (solid black line) exists only in an interval of values of $\Delta\omega > 0$. As the self-coupling terms are increased, Fig. 4(b) shows that the region of stable synchronization becomes broader, and invades negative values of $\Delta\omega$, see also Figs. 3(a)–3(d).

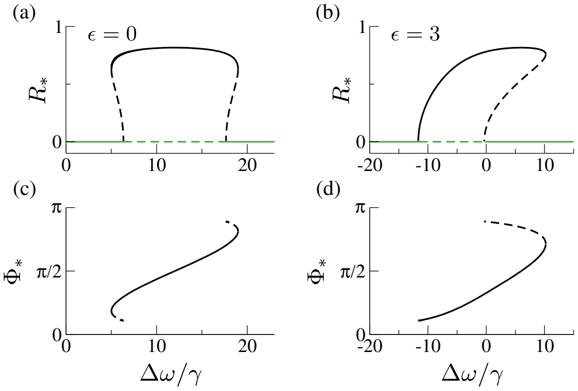

FIG. 4. Bifurcation diagrams of synchronized (black) and incoherent (green) states of Eqs. (17) for $K/\gamma = 6$, obtained using Eq. (18). (a), (b) Amplitude R_* and (c,d) phase difference Φ_* between the Kuramoto order parameters for (a), (c) $\epsilon = 0$ and (b), (d) $\epsilon = 3$.

Note that the phase difference Φ_* between Z_E and Z_I increases monotonically with $\Delta\omega$, see Figs. 4(c) and 4(d), but lies within the interval $(0, \pi)$, and thus excitation always precedes inhibition, see also Eq. (17).

Differentiating Eq. (18) with respect to R_*^2 and equating the result to zero, allows us to analytically obtain the red boundaries in Fig. 3 in parametric form (not shown), corresponding to saddle-node bifurcations. As $R_* \to 0$, these bifurcations meet the boundaries Eq. (11) at codimension-2 points where the instabilities change from sub- to supercritical. The exact value of the K coordinate is

$$(K/\gamma)_{c2}^{\pm} = \sqrt{(8 - 2\epsilon^2 \mp 2\epsilon\sqrt{8 + \epsilon^2})/(1 - \epsilon^2)}. \qquad (19)$$

Substituting these values into Eq. (11) with $D = 0$, we find the location of the codimension-two points represented in Fig. 3.

Finally, we have numerically verified that very similar bistability regions appear in the phase diagrams for the noisy *EI*-Kuramoto model Eq. (4) with identical oscillators ($D > 0$, $\gamma = 0$). In addition, following Ref. [58], we found that the codimension-2 points of the noisy *EI*-KM are located at [59]

$$(K/D)_{c2}^{\pm} = \sqrt{(12 - 2\epsilon^2 \mp 2\epsilon\sqrt{24 + \epsilon^2})/(1 - \epsilon^2)}, \qquad (20)$$

which is strikingly similar to Eq. (19), but here the points lie at slightly larger K values.

Conclusions.—Using the averaging approximation we derived a two-population Kuramoto model—that we call *EI*-KM—from an *EI*-network of pulse-coupled, Type 1 oscillators. The resulting *EI*-KM displays a transition to synchronization that has the main features of the *EI*-based (also known as PING, pyramidal-interneuron gamma) rhythms [17–24]: (i) Oscillations set in exclusively due to the cooperative action of both E and I populations; (ii) oscillations emerge if excitatory dynamics is faster than inhibition, irrespective of ϵ. (iii) Otherwise, when inhibition is faster than excitation, strong enough self-coupling ($\epsilon > 1$) is necessary for synchrony to occur. (iv) Excitation always precedes inhibition ($0 < \Phi_* < \pi$). (v) The transition between incoherence and synchronization is often hysteretic, see, e.g., Ref. [23]. While these results have been rigorously demonstrated in the *EI*-KM with Lorentzian heterogeneities (by means of the OA ansatz), perturbative and numerical analysis of the *EI*-KM with noise reveal the same global picture.

We acknowledge support by MINECO (Spain) under Projects No. FIS2016-74957-P, No. PSI2016-75688-P, and No. PCIN-2015-127. We also acknowledge support by the European Union's Horizon 2020 research and innovation programme under the Marie Skłodowska-Curie Grant Agreement No. 642563.

[1] Y. Kuramoto, *Chemical Oscillations, Waves, and Turbulence* (Springer-Verlag, Berlin, 1984).
[2] S. H. Strogatz, Physica (Amsterdam) **143D**, 1 (2000).
[3] A. S. Pikovsky, M. G. Rosenblum, and J. Kurths, *Synchronization, a Universal Concept in Nonlinear Sciences* (Cambridge University Press, Cambridge, England, 2001).
[4] J. A. Acebrón, L. L. Bonilla, C. J. Pérez-Vicente, F. Ritort, and R. Spigler, Rev. Mod. Phys. **77**, 137 (2005).
[5] A. Pikovsky and M. Rosenblum, Chaos **25**, 097616 (2015).
[6] K. Wiesenfeld, P. Colet, and S. H. Strogatz, Phys. Rev. Lett. **76**, 404 (1996).
[7] S. H. Strogatz, D. M. Abrams, A. McRobie, B. Eckhardt, and E. Ott, Nature (London) **438**, 43 (2005).
[8] I. Z. Kiss, Y. Zhai, and J. L. Hudson, Science **296**, 1676 (2002).
[9] G. Buzsáki, *Rhythms of the Brain* (Oxford University Press, New York, 2006).
[10] M. Breakspear, S. Heitmann, and A. Daffertshofer, Front. Hum. Neurosci. **4**, 190 (2010).
[11] J. Cabral, E. Hugues, O. Sporns, and G. Deco, NeuroImage **57**, 130 (2011).
[12] R. Ton, G. Deco, and A. Daffertshofer, PLoS Comput. Biol. **10**, e1003736 (2014).
[13] P. Villegas, P. Moretti, and M. A. Muñoz, Sci. Rep. **4**, 5990 (2014).
[14] A. Ponce-Alvarez, G. Deco, P. Hagmann, G. L. Romani, D. Mantini, and M. Corbetta, PLoS Comput. Biol. **11**, e1004100 (2015).
[15] P. Sanz-Leon, S. A. Knock, A. Spiegler, and V. K. Jirsa, NeuroImage **111**, 385 (2015).
[16] S. Petkoski, A. Spiegler, T. Proix, P. Aram, J.-J. Temprado, and V. K. Jirsa, Phys. Rev. E **94**, 012209 (2016).
[17] M. Whittington, R. Traub, N. Kopell, B. Ermentrout, and E. Buhl, Int. J. Psychophysiol. **38**, 315 (2000).
[18] P. Tiesinga and T. J. Sejnowski, Neuron **63**, 727 (2009).
[19] X.-J. Wang, Physiol. Rev. **90**, 1195 (2010).
[20] G. Buzsáki and X.-J. Wang, Annu. Rev. Neurosci. **35**, 203 (2012).
[21] H. R. Wilson and J. D. Cowan, Biophys. J. **12**, 1 (1972).
[22] N. Brunel and X.-J. Wang, J. Neurophysiology **90**, 415 (2003).
[23] D. Hansel and G. Mato, Neural Comput. **15**, 1 (2003).
[24] C. Boergers and N. Kopell, Neural Comput. **15**, 509 (2003).
[25] A. T. Winfree, J. Theor. Biol. **16**, 15 (1967).
[26] J. T. Ariaratnam and S. H. Strogatz, Phys. Rev. Lett. **86**, 4278 (2001).
[27] D. Pazó and E. Montbrió, Phys. Rev. X **4**, 011009 (2014).
[28] R. Gallego, E. Montbrió, and D. Pazó, Phys. Rev. E **96**, 042208 (2017).
[29] C. R. Laing, Physics **7**, 10 (2014).
[30] B. Ermentrout and N. Kopell, SIAM J. Appl. Math. **46**, 233 (1986).
[31] B. Ermentrout, Neural Comput. **8**, 979 (1996).
[32] E. M. Izhikevich, *Dynamical Systems in Neuroscience* (MIT Press, Cambridge, Massachusetts, 2007).
[33] E. Brown, J. Moehlis, and P. Holmes, Neural Comput. **16**, 673 (2004).
[34] Phase variables in Eq. (4) correspond to slow-phase approximations of the phases in Eq. (1); See Supplemental Material at http://link.aps.org/supplemental/10.1103/PhysRevLett.120.244101 for its derivation.
[35] H. Okuda and Y. Kuramoto, Prog. Theor. Phys. **86**, 1159 (1991).
[36] E. Montbrió, J. Kurths, and B. Blasius, Phys. Rev. E **70**, 056125 (2004).
[37] E. Barreto, B. Hunt, E. Ott, and P. So, Phys. Rev. E **77**, 036107 (2008).
[38] D. M. Abrams, R. Mirollo, S. H. Strogatz, and D. A. Wiley, Phys. Rev. Lett. **101**, 084103 (2008).
[39] Y. Kawamura, H. Nakao, K. Arai, H. Kori, and Y. Kuramoto, Chaos **20**, 043110 (2010).
[40] B. Pietras, N. Deschle, and A. Daffertshofer, Phys. Rev. E **94**, 052211 (2016).
[41] H. Sakaguchi and Y. Kuramoto, Prog. Theor. Phys. **76**, 576 (1986).
[42] Using $\phi_i^E \equiv \theta_i^E - \pi/2$, Eq. (4) transforms into a two-population model with phases $\{\phi_i^E\}$, $\{\theta_i^I\}$, where self-interaction functions remain the same, while cross-interaction functions become sine functions with the precise signs to favor synchrony. Hence, for the case $K_{EE} = K_{II} = 0$ considered in Fig. 2, the system reduces to a bipartite network of Kuramoto oscillators.
[43] S. H. Strogatz and R. E. Mirollo, J. Stat. Phys. **63**, 613 (1991).
[44] See Supplemental Material at http://link.aps.org/supplemental/10.1103/PhysRevLett.120.244101 for details.
[45] E. Ott and T. M. Antonsen, Chaos **18**, 037113 (2008).
[46] E. Ott and T. M. Antonsen, Chaos **19**, 023117 (2009).
[47] See Supplemental Material at http://link.aps.org/supplemental/10.1103/PhysRevLett.120.244101 for details, see also Ref. [28].
[48] See Supplemental Material at http://link.aps.org/supplemental/10.1103/PhysRevLett.120.244101 for the proof that, in the *EI*-KM, the mean field h_σ is linearly related with the *mean firing rate* of the population of oscillators, which, compared to h_σ, is a more natural measure of neuronal activity in neuroscience.

[49] See Supplemental Material at http://link.aps.org/supplemental/10.1103/PhysRevLett.120.244101 for the numerical demonstration.

[50] See Supplemental Material at http://link.aps.org/supplemental/10.1103/PhysRevLett.120.244101 for the proof.

[51] E. A. Martens, E. Barreto, S. H. Strogatz, E. Ott, P. So, and T. M. Antonsen, Phys. Rev. E **79**, 026204 (2009).

[52] In contrast with the KM with bimodal frequency distribution [1,40,51,53–56], our numerical simulations did not reveal states with time-varying R_{σ}. The same occurs in other variants of the KM, see, e.g., Ref. [57].

[53] J. D. Crawford, J. Stat. Phys. **74**, 1047 (1994).

[54] L. L. Bonilla, J. C. Neu, and R. Spigler, J. Stat. Phys. **67**, 313 (1992).

[55] E. Montbrió, D. Pazó, and J. Schmidt, Phys. Rev. E **74**, 056201 (2006).

[56] D. Pazó and E. Montbrió, Phys. Rev. E **80**, 046215 (2009).

[57] H. Hong and S. H. Strogatz, Phys. Rev. E **85**, 056210 (2012).

[58] A. Pikovsky and S. Ruffo, Phys. Rev. E **59**, 1633 (1999).

[59] See Supplemental Material at http://link.aps.org/supplemental/10.1103/PhysRevLett.120.244101 for the analytical derivation.